J. Fluid Mech. (1994), *vol.* 267, *pp.* 83–108

Nonlinear modulations of solitary waves

By GEIR PEDERSEN

Department of Mechanics, University of Oslo, PO Box 1053, Blindern, 0316 Oslo, Norway

(Received 24 December 1992 and in revised form 4 November 1993)

The leading optical approximation to a slowly varying solitary crest on constant depth is the plane soliton solution with the local values of amplitude and orientation substituted. This leads to two nonlinear hyperbolic equations for the local amplitude and inclination of the crest that have been reported by several authors and predict the formation of progressive wave jumps, or shocks, from any initial perturbation of the crest. In comparison to numerical solutions of the Boussinesq equations we find that this optical approximation fails to reproduce essential properties of the crest dynamics, in particular that the crest modulations are damped and that well-defined wave jumps do not necessarily evolve. One purpose of the present work is to include such features in an amended optical approximation.

We obtain the leading correction to the 'local soliton' solution by a multiple scale technique. In addition to a modification to the wave profile the perturbation expansion also yields a diffracted wave system and a celerity that depends on the curvature of the crest. The principle of energy conservation then leads us to a second-order optical approximation consisting of transport equations of mixed hyperbolic/parabolic nature. Under additional assumptions the transport equations can be reduced to the well-known Burgers equation.

Numerical simulations of the Boussinesq equations are performed for modulations on otherwise straight crests and radially converging solitons. The improved optical, or ray, theory reproduces all essential features and agrees closely with the numerical solution in both cases. Contrary to purely hyperbolic optical descriptions the present theory also predicts wave jumps of finite width that are consistent with the triad solution of Miles (1977).

The present work indicates that while sinusoidal waves often are appropriately described by the lowest-order physical optics, higher-order corrections must be expected to be important for single crested waves.

1. Introduction

Approximate theories for wave propagation in a slowly varying medium are most extensively developed and applied for linear, harmonic waves. However, there has also been some progress for particular species of nonlinear waves such as shock waves (Whitham 1974), Stokes-type waves (Peregrine 1985) and shallow-water solitons (Miles 1980) which are the concern of the present work.

Seismic activity, submarine slides, rock and snow avalanches into lakes etc. may generate devastating systems of huge waves. In coastal waters these may be headed by one or more crests of a form akin to solitary waves. Hence, insight into the dynamics of non-uniform solitary crests may be helpful for the understanding of tsunami propagation and impact on shore. The larger part of the reported work

on modulated solitons has been directed towards waves normally incident on a shelf or propagating in a narrow channel of gently varying width. However, there has also been some activity on genuine three-dimensional problems, generally through application of simple optical methods. Kulikovskii & Reutov (1976, 1980) studied solitons in variable depths and over underwater trenches and ridges. Reutov (1976) and Miles (1977*c*) discuss the behaviour of non-uniform solitary crests on constant depth. One of the major results is the existence of laterally moving disturbances that eventually develop shocks. Analogues shocks, or wave jumps, are known also for other nonlinear waves (Yue & Mei 1980; Peregrine 1983; Liu & Yoon 1986). For shallow-water solitons Miles (1977*b*) gives a complete description of such jumps in the form of phase-locked triads, presented in the context of Mach reflection. Herein we will investigate the dynamics of a solitary crest both through general numerical solutions and a new optical theory.

A direct derivation of an optical theory for solitons by application of the phase velocity–amplitude relation and the usual assumptions concerning energy transport is straightforward. Grimshaw (1970) developed transport equations by means of a formal multiple scale expansion on a set of two-dimensional Boussinesq-type equations. In 1971 he generalized the expansion to three dimensions, starting this time from the full inviscid description. Later Ko & Kuehl (1979) applied a similar method for radially converging or diverging ion acoustic waves in two and three dimensions. In the present paper we investigate the dynamics of a soliton-like crest in constant depth, with the combined purpose of getting insight into the physics as well as the performance of the optical approaches. We find that the standard optical theory, as described by Miles (1977*c*), Reutov (1976) and others, displays severe shortcomings when compared to numerical solutions of the Boussinesq equations. This is the main motivation for the construction of the higher-order ray theory that is to be presented in §3. The corrected transport equations are found by combining a formal perturbation expansion and energy arguments. The expansion is intimately related to the one reported by Grimshaw, but is amended in several ways to obtain suitable representations of the higher-order terms. When the corresponding modified wave field replaces the 'local soliton' approximation in the energy balance considerations we then arrive at an improved energy transport equation. A higher-order kinetic equation, on the other hand, follows directly from the perturbation technique. Together these two transport equations form an optical approximation that possesses important new properties and reproduces full solutions closely in several examples. In the present context the term 'full' means that no assumption of slow variation has been invoked and we employ both numerical solutions of the Boussinesq equations and Miles' (1977*b*) analytical solution for a resonant triad of solitons.

2. Basic equations

Marking dimensional quantities by a star we introduce a coordinate system with horizontal axes $ox^\star$, $oy^\star$ in the undisturbed water level and $oz^\star$ pointing vertically upwards. Further we assume a flat bottom at $z^\star = -h^\star$ and apply $h^\star$ and $(gh^\star)^{\frac{1}{2}}$ as characteristic length and speed respectively. We are then led to the following definition of non-dimensional variables:

$$\left.\begin{aligned} x^\star &= h_0^\star x, \quad & y^\star &= h_0^\star y, & t^\star &= h_0^\star (gh_0^\star)^{-\frac{1}{2}} t, \\ \eta^\star &= h_0^\star \eta, \quad & \phi^\star &= h_0^\star (gh_0^\star)^{\frac{1}{2}} \phi, & z^\star &= h_0^\star z, \end{aligned}\right\} \tag{2.1}$$

where η is the surface elevation and ϕ is the velocity potential.

In terms of η and the averaged potential $\overline{\phi}$ the Boussinesq equations can be written

$$\eta_t = -\nabla \cdot \{(1+\eta)\nabla\overline{\phi}\}, \tag{2.2}$$

$$\overline{\phi}_t + \eta + \tfrac{1}{2}(\nabla\overline{\phi})^2 - \tfrac{1}{3}\nabla^2\overline{\phi}_t = 0. \tag{2.3}$$

A derivation of these equations can be found in Wu (1981).

For the soliton solution we write

$$\eta = AY(\chi, A), \quad \overline{\phi} = B\Phi(\chi, A), \tag{2.4}$$

where A is a measure of the amplitude and the linear phase function is defined as $\chi = k(\boldsymbol{n}\cdot\boldsymbol{r} - c_0 t)$ in which $\boldsymbol{n}$ is the unit vector in the direction of wave advance. The exact soliton solution (of the fully inviscid equations) can be expressed through power series in A according to

$$\left.\begin{aligned} Y &= Y_0 + \tfrac{3}{4}AY_0^2 + \dots, & \Phi_\chi &= Y_0 - \tfrac{1}{4}AY_0^2 + \dots, \\ k &= \tfrac{1}{2}(3A)^{\frac{1}{2}}(1 + k_1 A + \dots), & c_0 &= 1 + \tfrac{1}{2}A + c_2A^2 + \dots, \\ B &= c(A/k), & E &= (8/3^{\frac{3}{2}})A^{\frac{3}{2}}(1 + \tfrac{33}{20}A + \dots), \end{aligned}\right\} \tag{2.5}$$

where $Y_0(\chi) = \operatorname{sech}^2(\chi)$ and E is the integrated energy content of the soliton. The second-order terms for Y, Φ and E are obtained from Laitone (1960) and Longuet-Higgins & Fenton (1974). Naturally, the soliton solution of the Boussinesq equations will agree with the above expressions for Y, Φ and E only to the leading order in A. A brief summary as to when and by whom the different terms of the expansion (2.5) were first reported is found in Witting (1975).

3. Transport equations for a slowly modulated crest

We will be dealing with wave patterns consisting of a single, nearly soliton shaped, crest as primary wave field and a secondary, or residual, system of diffracted waves. Whenever possible the x-axis will be aligned parallel to the main direction of wave advance for the primary wave and the field variables evaluated at the crest peak will be marked by the superscript $^{(m)}$.

3.1. *The corrected wave field*

We assume that the variation rate of height and orientation of the principal crest can be quantified by the small parameter β, which leads to the introduction of slow variables $(\hat{x}, \hat{y}, \hat{t}) = \beta(x, y, t)$. A perturbed soliton-like crest is written as

$$\left.\begin{aligned} \eta &= AY(\chi, A) + \beta\hat{\eta}(\chi, \hat{x}, \hat{y}, \hat{t}) + O(\beta^2), \\ \overline{\phi} &= B\Phi(\chi, A) + \beta\hat{\phi}(\chi, \hat{x}, \hat{y}, \hat{t}) + O(\beta^2), \end{aligned}\right\} \tag{3.1}$$

where A is a function of the slow variables and the form functions Y and Φ are as defined in (2.5). We note that the slow variables enter the expressions for Y and Φ only implicitly through A. Grimshaw (1970, 1971), as well as Ko & Kuehl (1978, 1979), introduced a multiplicative factor depending on slow variables, before the phase function (see Appendix A). The phase function χ, which represents the fast variation, is no longer linear. Hence, the wavenumber, $\boldsymbol{k}$, and phase speed, c, defined by

$$\boldsymbol{k} = \nabla\chi, \quad kc = -\chi_t, \quad k = |\boldsymbol{k}|, \tag{3.2}$$

are functions of the independent variables. Contrary to Grimshaw and Ko & Kuehl we expand the phase speed and wavenumber (see Appendix A) according to

$$c = c_0 + \beta(c_1^{(1)}(\hat{x}, \hat{y}, \hat{t})\chi + c_1^{(0)}(\hat{x}, \hat{y}, \hat{t})) + O(\beta^2), \tag{3.3}$$

$$\boldsymbol{k} = \boldsymbol{k}_0 + \beta(S^{(1)}(\hat{x}, \hat{y}, \hat{t})\chi + S^{(0)}(\hat{x}, \hat{y}, \hat{t}))\boldsymbol{s} + O(\beta^2), \tag{3.4}$$

where c_0 and $k_0 = |\boldsymbol{k}_0|$ relate to A as described in (2.5). Defining $\boldsymbol{n} \equiv \cos\theta\boldsymbol{i} + \sin\theta\boldsymbol{j}$ as the unit vector parallel to $\boldsymbol{k}_0$ we may further define $\boldsymbol{S} = \boldsymbol{i}_z \times \boldsymbol{n}$. Leaving the details for Appendix A we arrive at the energy transport equation

$$(A^{\frac{3}{2}})_{\hat{t}} + c_0\hat{\nabla} \cdot (\boldsymbol{n}A^{\frac{3}{2}}) = O(A^{\frac{7}{2}}). \tag{3.5}$$

The equation is easily brought into standard conservative form, but this is really inadequate since it, by itself, expresses energy conservation in an integrated sense only. The phase speed corrections read

$$c_1^{(1)} = (3A)^{-\frac{1}{2}}(-A_{\hat{n}} + \tfrac{2}{3}\theta_{\hat{s}}) + O(A^{\frac{1}{2}}), \tag{3.6}$$

$$c_1^{(0)} = -(3A)^{-\frac{1}{2}}\theta_{\hat{s}} + O(A^{\frac{3}{2}}), \tag{3.7}$$

where the subscripts $\hat{s}$ and $\hat{n}$ denote differentiation in the $\boldsymbol{s}$- and $\boldsymbol{n}$-directions respectively. We note that the correction to the phase speed at the peak is proportional to the curvature of the principal crest. For the first-order wave field we may write

$$\hat{\eta} = \tfrac{2}{3}(3A)^{-\frac{1}{2}}\theta_{\hat{s}}\Phi_0 + 2c_1^{(1)}(\chi Y_0 + \tfrac{1}{4}\chi^2 Y_{0,\chi}) + O(A^{\frac{3}{2}}), \tag{3.8}$$

$$\hat{\phi} = k_0^{-1}c_1^{(1)}(\chi\Phi_0 + \tfrac{1}{2}\chi^2 Y_0) + O(A), \tag{3.9}$$

where $\Phi_0 \equiv \int_\infty^\chi Y_0 d\chi = 1 - \tanh\chi$. From the above expression for $\hat{\phi}$ and (3.1) we obtain a non-zero cross-ray velocity, defined as the component along $\boldsymbol{s}$, that becomes important for the subsequent energy considerations (see discussion below (3.15)). For the position of the primary crest ($\chi = 0$) we may now write the kinematic equation

$$x_t^{(m)} = \cos^{-1}\theta^{(m)}(c_0 + \beta c_1^{(0)})^{(m)}. \tag{3.10}$$

The equations (3.7) and (3.8) imply that a converging, or focusing, crest ($\theta_{\hat{s}} < 0$) has an increased propagation velocity and is followed by a surface elevation, whereas a diverging wave is retarded and followed by a trough. As a consequence, the modification $c_1^{(0)}$ to the wave speed will tend to straighten a crest that inherits alternating focusing and defocusing regions.

Behind the primary wave ($\chi \to -\infty$) Y and Φ_χ decay exponentially, whereas $\Phi_0 \to -2$. Consequently the downstream wave field does not vanish, but is defined through

$$\eta_{-\infty} = -\tfrac{4}{3}\beta(3A)^{-\frac{1}{2}}\theta_{\hat{s}}, \quad \boldsymbol{v}_{-\infty} = -\beta(3A)^{-\frac{1}{2}}(\tfrac{4}{3}\theta_{\hat{s}}\boldsymbol{n} + 2A_{\hat{s}}\boldsymbol{s}), \tag{3.11}$$

where $\boldsymbol{v}_{-\infty}$ is the particle velocity and relative errors of order A, β are implicit throughout. If (3.1) together with (3.8) and (3.9) define a uniform solution the above wave field has to fulfil the linear hydrostatic equations to the leading order in A and β. Assuming $A_{\hat{n}} = 0$, say, we obtain anyway a local solution for the vicinity of $x^{(m)}$ that can be matched to an outer wave field to give a complete solution. In some cases we are able to construct uniform solutions with $c_1^{(1)} = 0$ which correspond to very compact representations of the field variables.

3.2. *Integrated conservation laws*

Higher-order counterparts to (3.5) can in principle be found by going to higher orders in the perturbation scheme. However, the energy equation (3.5) can readily be recast

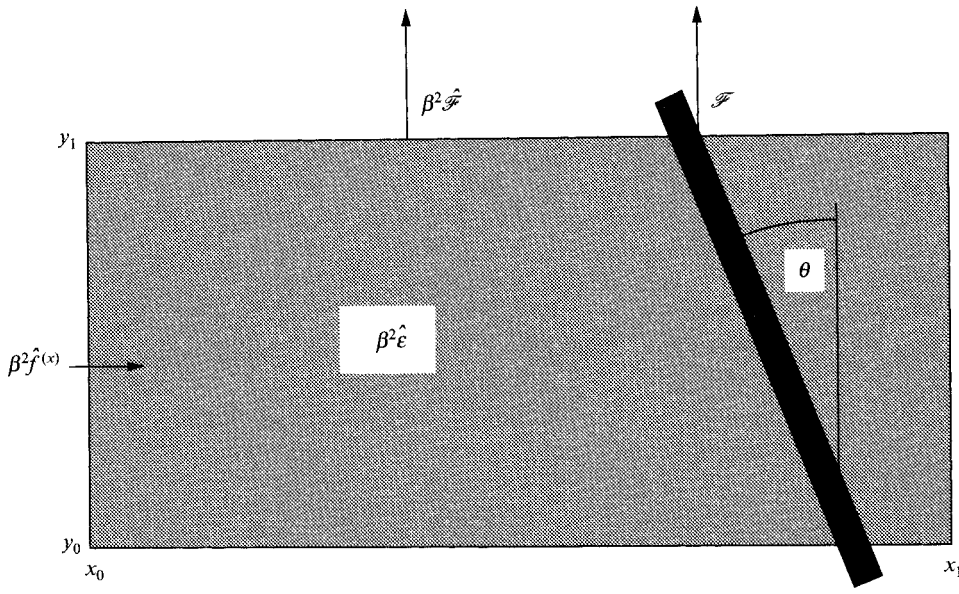

FIGURE 1. Control volume for energy account. The volume corresponds to the shaded region, while the fat solid line represent the primary wave.

into the energy equation employed by Miles (1977*c*) and others, that alternatively can be deduced by a direct energy balance argument applied to the primary wave field only. Correspondingly, similar arguments applied to the corrected wave field will result in a higher-order integrated energy equation. As compared to advancing the perturbation scheme this will constitute a simpler and altogether more illustrative approach.

A control volume for energy balance is depicted in figure 1 where $\mathscr{F}$ is the total energy flux in the y-direction associated with the primary crest, $\beta^2\hat{\varepsilon}$, $\beta^2\hat{f}^{(x)}$, $\beta^2\hat{f}^{(y)}$ the energy and energy-flux densities of the diffracted field and $\hat{\mathscr{F}}$ denotes the integral of $\hat{f}^{(y)}$. Further, for the flux and density integrated across the stem we invoke the partition: $\mathscr{F} = \mathscr{F}_0 + \beta\mathscr{F}_1$, $\mathscr{E} = \mathscr{E}_0 + \beta\mathscr{E}_1$. The first-order parts are associated with products between the $O(1)$ and $O(\beta)$ field variables and variations of A, $\boldsymbol{k}$ and c across the crest. However, the latter contribution turns out to be zero. Letting $y_1 - y_0 \to 0$ we now obtain an integrated conservation law in ordered form:

$$\mathscr{E}_{0,\hat{t}} + \beta\mathscr{E}_{1,\hat{t}} = -\mathscr{F}_{0,\hat{y}} - \beta\mathscr{F}_{1,\hat{y}} - \beta\mathscr{D} + O(\beta^2), \tag{3.12}$$

$$\mathscr{D} = -\left(\hat{f}^{(x)} + \tan\theta^{(m)}\hat{f}^{(y)} - \frac{c^{(m)}}{\cos\theta^{(m)}}\hat{\varepsilon}\right) + O(\beta^2), \tag{3.13}$$

where $\mathscr{D}$ can be interpreted as the energy leak due to the diffracted wave field.

The integrands in the expressions for $\mathscr{E}_0$ and $\mathscr{F}_0$ are symmetric in χ and decay exponentially at the outskirts of the primary wave. In these integrals the effect of slow variations will thus cancel to $O(\beta)$. Owing to these observations the integration is straightforward and we arrive at

$$\mathscr{E}_0 = \frac{E(A^{(m)})}{\cos\theta^{(m)}}, \quad \mathscr{E}_1 = -\frac{16\theta_{\hat{s}}^{(m)}}{9\cos\theta^{(m)}} + O(A^2), \tag{3.14}$$

where $E(A)$ is the energy of a straight soliton of amplitude A integrated over a

cross-section normal the crest. For the vertically integrated flux density we find

$$\boldsymbol{f} = (f_0 + \beta f_1)\boldsymbol{n} + 3^{-\frac{1}{2}}\beta A^{\frac{1}{2}} A_{\hat{s}} \Phi_0 Y_0 \boldsymbol{s} + O(\beta^2, \beta A^{\frac{5}{2}}), \tag{3.15}$$

where $f_0\boldsymbol{n}$ is the contribution from the primary wave. The last term corresponds to a cross-ray energy transport. Physically, this transport stems from the lateral pressure gradient that necessarily is present under a ridge of variable height and produces lateral accelerations which integrate to a lateral velocity component. The dominant part of the cross-ray energy flux then corresponds to the work exerted by the pressure against this velocity. These arguments are easily quantified to enable a direct calculation of the last term of (3.15) as well as the s-component of the total velocity, without application of the formal perturbation expansion. Unfortunately, the other $O(\beta)$ terms cannot be obtained in a similar manner. Integrating the term $f_0 \sin\theta^{(m)}$ we obviously obtain $c_0^{(m)}\mathscr{E}_0 \tan\theta^{(m)}$ owing to the consistency of the plane soliton solution. Through integration of the remaining terms in (3.15) we find a corresponding relation between $\mathscr{E}_1$ and the integral of f_1 and arrive at

$$\mathscr{F}_0 + \beta\mathscr{F}_1 = c_0^{(m)}(\mathscr{E}_0 + \beta\mathscr{E}_1)\sin\theta^{(m)} - \beta\tfrac{4}{3}A_{\hat{s}}^{(m)} + O(\beta^2, \beta A^2). \tag{3.16}$$

The term $\beta c_1^{(0)}\mathscr{E}_0 \sin\theta^{(m)}$ does not show up because it is of higher order in A.

The surface elevation and velocity immediately behind the primary wave are found by putting $x = x^{(m)}$ in (3.11). When these field quantities are substituted into (3.13) we find that the leading-order terms in A cancel out and we obtain

$$\mathscr{D} = \left(\frac{8(\theta_{\hat{s}}^{(m)})^2}{27} + \frac{2(A_{\hat{s}}^{(m)})^2}{3A^{(m)}}\right)\frac{1}{\cos\theta^{(m)}}\,. \tag{3.17}$$

One might object that higher-order corrections to $\hat{\eta}$ and $\hat{\phi}$ may be important owing to the nihilation of leading contributions to $\mathscr{D}$. However, a careful examination of the calculation leading to (3.17) reveals that this is not the case. We further note that the quantity $\cos\theta^{(m)}\mathscr{D}$, which is independent of the orientation of the coordinate axes, can be recognized as the energy leak density measured per length of the principal crest.

Summarizing the above results we find the improved energy equation

$$\left(\frac{E}{\cos\theta^{(m)}} - \tfrac{16}{9}\beta\theta_{\hat{y}}^{(m)}\right)_{\hat{t}} = -\left(c_0\tan\theta^{(m)}E - \tfrac{16}{9}\beta\sin\theta^{(m)}\theta_{\hat{y}}^{(m)} - \tfrac{4}{3}\beta\cos\theta^{(m)}A_{\hat{y}}^{(m)}\right)_{\hat{y}}$$
$$-\frac{\beta}{\cos\theta^{(m)}}\left(\frac{8(\theta_{\hat{y}}^{(m)})^2}{27} + \frac{2(A_{\hat{y}}^{(m)})^2}{3A^{(m)}}\right). \tag{3.18}$$

Using a similar analysis we have found that the preceding results are consistent with conservation of volume and momentum. In addition we obtain the relation

$$\boldsymbol{n}\cdot\boldsymbol{v}_{-\infty} - \eta_{-\infty} = -\tfrac{3}{2}A^{(m)}\eta_{-\infty}(1 + O(A)), \tag{3.19}$$

that is valid for $x = x^{(m)}$ and where $\eta_{-\infty}$ and $\boldsymbol{v}_{-\infty}$ are defined as in (3.11).

3.3. *Gently modulated crests*

For small modulations on a straight crest we may assume $\theta^{(m)}$ small. Using (3.10) and representing E and c_0 to the leading order in $A^{(m)}$ we obtain

$$\{(A^{(m)})^{\frac{3}{2}}\}_{\hat{t}} = -\{(A^{(m)})^{\frac{3}{2}}\theta^{(m)}\}_{\hat{y}} + \frac{3^{-\frac{1}{2}}\beta}{2}A_{\hat{y}\hat{y}} - \beta\frac{(\theta_{\hat{y}}^{(m)})^2}{3^{\frac{3}{2}}} - \beta\frac{3^{\frac{1}{2}}(A_{\hat{y}}^{(m)})^2}{4A^{(m)}}\,, \tag{3.20}$$

from the energy equation (3.2). The second term on the right-hand side has a form akin to the diffusion term of the standard heat equation, whereas the last term represents an energy sink. Using the same terminology we may classify the first term on the right-hand side as an advection term, with $\theta^{(m)}$ in the role of velocity. The corresponding kinematic equation is readily obtained from (3.10):

$$\theta^{(m)}_{\hat{t}} = -\tfrac{1}{2}(A^{(m)} + (\theta^{(m)})^2)_{\hat{y}} + \beta\{(3A^{(m)})^{-\frac{1}{2}}\theta^{(m)}_{\hat{y}}\}_{\hat{y}}\,. \tag{3.21}$$

Again the corrections of higher order in β give rise to a term reminiscent of diffusion in an otherwise hyperbolic equation. Naturally, the errors due to the omission of higher-order terms (in A) in E and c_0 will often be larger than the $O(\beta)$ terms in the above transport equations (3.20) and (3.21). However, it will still be appropriate to retain the latter terms since they introduce qualitatively new mathematical features. In fact, each term in (3.20) and (3.21) can be regarded as the leading representation of a particular physical effect. A tendency toward formation of wave jumps, due to the nonlinear 'advective' terms in the transport equations, is now opposed by the diffusion-like effect of cross-ray energy transport and the dependencies of energy density and propagation velocity upon the curvature of the primary crest.

To leading order in β we may easily recast (3.20) and (3.21) into characteristic form according to

$$\frac{\mathrm{d}}{\mathrm{d}t}((3A^{(m)})^{\frac{1}{2}} \pm \theta^{(m)}) = 0 \quad \text{at } C^{\pm} : \frac{\mathrm{d}y}{\mathrm{d}t} = \theta^{(m)} \pm \left(\frac{A^{(m)}}{3}\right)^{\frac{1}{2}}, \tag{3.22}$$

which is equivalent with the description employed by, for instance, Miles (1977*c*).

Under the assumption that all disturbances move along the C^+ characteristic, as defined above, the ray description (3.20) and (3.21) can be substantially simplified. We further assume that the absolute variation in A is of order β, which implies that the leading nonlinearities (in a as defined below) in the 'advective' terms of the ray equations are comparable to the 'diffusion' like terms. Consequently, we change variables according to

$$A^{(m)} = A_0(1 + \beta a), \quad \theta^{(m)} = \beta A_0^{\frac{1}{2}}\psi, \quad \tilde{y} = A_0(\hat{y} - U\hat{t}), \tag{3.23}$$

where $U = (A_0/3)^{\frac{1}{2}}$ is introduced according to (3.22). In this frame of reference we may assume that the time dependence can be represented by the second-order slow variable

$$\tau = \beta U A_0 \hat{t} = \beta^2 U A_0 t. \tag{3.24}$$

Inserting the new variables into (3.20) and (3.21) we obtain a Burgers' equation for a:

$$a_\tau + (a^2)_{\tilde{y}} - \tfrac{2}{3}a_{\tilde{y}\tilde{y}} = O(\beta). \tag{3.25}$$

We note that the leakage term has dropped out of the equation to the present order.

Using the notations and assumptions inherent in (3.23) we may also find uniform solutions for η and $\overline{\phi}$ defined by $c_1^{(1)} = 0$ and

$$\left.\begin{aligned} A = A_0(1 + \beta(a^+(\zeta^+) + a^-(\zeta^-))), \quad \theta = \tfrac{1}{2}(3A_0)^{\frac{1}{2}}\beta(a^+(\zeta^+) - a^-(\zeta^-)), \\ \zeta^{\pm} = A_0(\hat{y} \mp U\hat{t}) \pm U(\hat{x} - c_0(A_0)\hat{t}), \end{aligned}\right\} \tag{3.26}$$

that for arbitrary functions $a^{\pm}$ fulfil (3.20), (3.21), (A 3) and (A 4) to the leading order in β. Substituting these expressions into (3.8) and (3.9) we observe that the diffracted wave field is a solution of the linear hydrostatic equations and consists

of two families of plane waves. The two systems have phase lines aligned at angles $\pm(3A_0)^{\frac{1}{2}}$ relative to the primary crest and are linked to perturbations propagating along the $C^{\pm}$ characteristics in (3.22) respectively. We note that the diffracted waves also are consistent with (3.19). The typical lengthscale of the diffracted waves is of order β^{-1}. When higher-order terms are taken into account, as in (3.25), the shape of the diffracted wave will evolve at a rate of order β^2. Thus, the diffracted wave field may be regarded as a slowly varying solution of the linear hydrostatic equations.

3.4. *Radially converging waves*

The axisymmetric case cannot inherit the diffusion-like features of the nearly straight crests discussed in the previous subsection. However, both the energy density and the wave celerity do still depend on the gradient of θ and the energy leak due to diffracted waves will also remain. The energy transport equation may now be formulated simply as a balance between energy loss in the principal wave and energy accumulated in the trailing wave system that is continuously prolongated. Integration in time then yields

$$r^{(m)}E(A^{(m)}) = r_0E(A_0) + \frac{8}{27}\ln\frac{r^{(m)}}{r_0}, \tag{3.27}$$

where r is the distance from the point of symmetry and $r^{(m)} = r_0$, $A^{(m)} = A_0$ define a reference state. To leading order in A the contribution to the total energy from $\mathscr{E}_1$ is constant and therefore drops out of the above equation. The equation (3.27) is described exclusively in terms of fast variables with $r^{(m)}$ itself as the ordering parameter. This reflects that the underlying perturbation expansion is asymptotically valid for large r. As the wave approaches the point of symmetry the right-hand side of (3.27) is bound to change sign for some $r^{(m)}$ and the equation loose sense. However, the whole asymptotic solution will become invalid long before this point is reached.

Ko & Kuehl (1979) reported an amplitude evolution that is consistent with having the logarithmic term of (3.27) multiplied by $r^{(m)}$. This leads to meaningless results and is certainly due to a misprint.

As opposed to the case of gently perturbed crests, the curvature dependence in the energy density introduces no principally new features in the final energy equation (3.27). This would probably still be the case even if $\mathscr{E}_1$ was calculated to the next order in A. We are then left with the energy loss to the diffracted tail as the genuine first-order effect in β. This effect is generally very small and may be important only when accumulated over an extremely large propagation distance (see figure 9). We note that for small A the equation (3.27) applies equally well when A is replaced by the total wave height, $\eta_{\max} \equiv \max(AY + \beta\hat{\eta})$. The explanation is simply that to the appropriate order we have $r^{(m)}(A^{(m)})^{\frac{3}{2}} - r^{(m)}(\eta_{\max})^{\frac{3}{2}} = \text{const.}$

Concerning the wave profile for radially symmetric waves we employ two representations of A. Setting $A = A^{(m)}$ we obtain a local solution that yields a non-zero $c_1^{(1)}$ and a form of (3.8) akin to the solution of Ko & Kuehl. Apart from two extra terms the corresponding expression of Ko & Kuehl can now be rewritten as (3.8). In addition to the term $D_1Y_{0,\chi}$ (see Appendix A) the solution of Ko & Kuehl also contains a term of type (A 6) corresponding to a redefinition of the amplitude: $A_1 = -4/(3r^{(m)}(3A^{(m)})^{\frac{1}{2}})$. When this amplitude modification is taken into account we find that the results of Ko & Kuehl also become consistent with $c_1^{(0)}$ as given in (3.7).

Alternatively, the expression

$$A = \frac{2(\hat{r} + \hat{t} + \hat{t}_0)}{3\hat{r}} \tag{3.28}$$

solves the transport equations to the appropriate order giving $c_1^{(1)} = 0$ and correct behaviour of the trailing wave. A singularity ahead of the principal crest and the large values of A attained as $\hat{r} \to \infty$ are of minor importance.

4. Examples

We will study the evolution of inhomogeneous solitary crests for three particular cases. Each case is analysed by the present optical theory as well as another method that involves no assumption of slow variation. In addition to the description of the primary crest, represented by $\theta^{(m)}$ and $A^{(m)}$, we will pay attention to the diffracted wave fields as well as the energy flux distributions.

First we study a progressive perturbation corresponding to a self-similar solution of the Burgers equation (3.25) that describes the evolution of the junction between two dislocated, but otherwise identical, semi-infinite crests. This solution is compared to numerical solutions of the Boussinesq equations and the set (3.20) and (3.21).

The second example is a wave jump of permanent form for which we compare results from the ray description to the general solution for a triad of solitons reported by Miles (1977*b*).

Finally we investigate a crest with radial symmetry. Mathematically this is a one-dimensional problem for which we may compute very accurate numerical solutions of the Boussinesq equations, permitting discussion of quantities like $c_1^{(0)}$. Since the ray theory in this case can be regarded as an asymptotic approximation for large r, in-going waves provide well-suited test examples for which the basic assumptions become gradually strained as $r^{(m)}$ diminishes with time.

4.1. *A self-similar perturbation – comparison to the Boussinesq solution*

The numerical procedure for solution of the Boussinesq equations differs from the one applied in Pedersen (1988) only with regard to minor, technical details. Consequently, we omit the description of the method. The ability of the method to represent solitary waves was studied by Pedersen (1991), who demonstrated the existence of discrete solitary waves expressible as single-crested permanent-form solutions of the difference equations. This is important in the present context where both length and time scales for the development of wave patterns may be very large and even a slight spurious damping or disintegration may corrupt the results. For completeness we sketch the numerical solution of (3.20) and (3.21) in Appendix B. To enable comparison with ray theory some secondary unknowns have to be calculated from the discrete Boussinesq solution. Energy fluxes are found by numerical integration of discrete counterparts of the expression

$$\boldsymbol{f} = -\overline{\phi}_t(1+\eta)\nabla\overline{\phi}(1+O(A^2)). \tag{4.1}$$

The quantities $A^{(m)}$ and $x^{(m)}$ are determined by the extremes of interpolating splines defined along grid rows parallel to the x-axis, thereby introducing a series of new approximations. However, in the present subsection the effects of these are negligible. The angle of orientation, $\theta^{(m)}$, is found by a polynomial (usually cubic) least-square fit to the interpolated extremes. Since the position of a maximum is sensitive to errors this procedure may sometimes produce visible artificial fluctuations, but generally not to an extent that affects the interpretation of the results.

We will add a few further comments on the wave patterns predicted by the Boussinesq equations. As stated in Appendix A the Boussinesq equations reproduce $\hat{\eta}$, $\hat{\phi}$ and c_1 correctly to the leading order in A. Also the leading balance of (3.2),

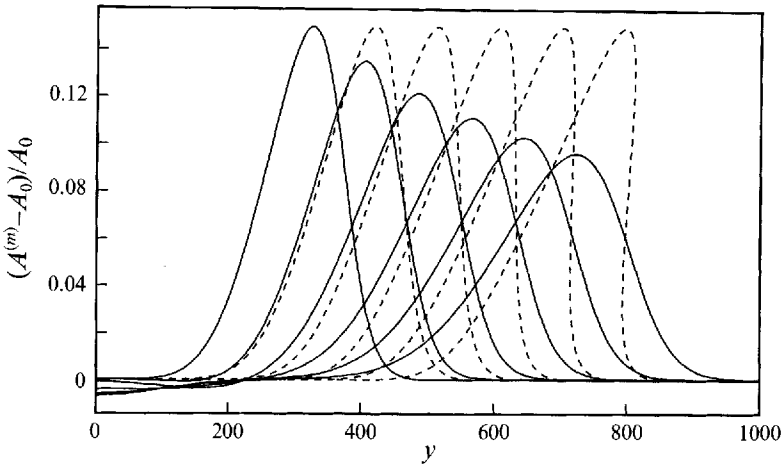

FIGURE 2. Time evolution of the initial condition (4.2), $t = 0$, with parameters $A_0 = 0.1$, $\Delta_{\max} = 0.15$ and $L = 66.7$. The selected times are $t = 0, 400, 800, ..., 2000$. The dashed lines correspond to the solution of the characteristic equations (3.22), whereas the numerical solution of the Boussinesq equations is depicted with solid lines.

that may be derived directly from (3.5), is inherent in this description. However, since the Boussinesq equations are not exactly energy conserving the corrected energy equation (3.20) cannot automatically be anticipated to apply to their solutions. Still, we would expect improved agreement from the higher-order transport equations as we indeed will observe. The initial conditions are derived from an initial distribution of $A^{(m)}$ and $\theta^{(m)}$ by substituting a phase function $\chi_{in}(x, y) \equiv k^{(m)} \cos\theta^{(m)}(x - x^{(m)})$ into the exact soliton solution for the actual Boussinesq equations. This solution is given in Pedersen (1988). Consequently, neither the full spatial variation of A and θ nor the $O(\beta)$ wave field are present in the initial state, but evolve over time. The fact that the secondary wave field is spontaneously induced over time increase its value as evidence for the ray theory.

The Burgers equation can be transformed to the linear heat equation by means of the Cole–Hopf transformation. Both the equation itself, the transformation and a selection of analytical solutions are discussed in detail by Whitham (1974). Here we will employ a self-similar solution that can be expressed in the variables y and t according to

$$\left.\begin{aligned} \frac{A^{(m)} - A_0}{A_0} &= \frac{\Delta_{\max}(t/t_0 + 1)^{-\frac{1}{2}} \exp(\sigma_{\max}^2 - \sigma^2)}{1 + \frac{3}{2}A_0 L(\ln 2)^{-\frac{1}{2}} \Delta_{\max} \exp(\sigma_{\max}^2)\,(\operatorname{erf}(\sigma_{\max}) - \operatorname{erf}(\sigma))}, \\ \sigma &= \frac{(\ln 2)^{\frac{1}{2}}(y - Ut)}{L(t/t_0 + 1)^{\frac{1}{2}}}, \quad t_0 = \frac{3(3A_0)^{\frac{1}{2}}L^2}{8\ln 2}, \quad \sigma_{\max} = \frac{3A_0 L}{4(\ln 2)^{\frac{1}{2}}}\Delta_{\max}, \end{aligned}\right\} \tag{4.2}$$

where U is as defined below (3.23) and erf denotes the error function. The solution contains two free parameters: $\Delta_{\max}$ which is the maximum initial relative perturbation of the amplitude, attained at $\sigma = \sigma_{\max}$, and L which is a measure of the initial lateral extension of the perturbation.

In figure 2 we have depicted the solutions of the characteristic equations (3.22) and the Boussinesq equations for initial conditions corresponding to (4.2) with $A_0 = 0.1$, $\Delta_{\max} = 0.15$ and $L = 66.7$. Although there is good agreement for the propagation speed of the disturbance, the different qualitative behaviour of the two solutions is

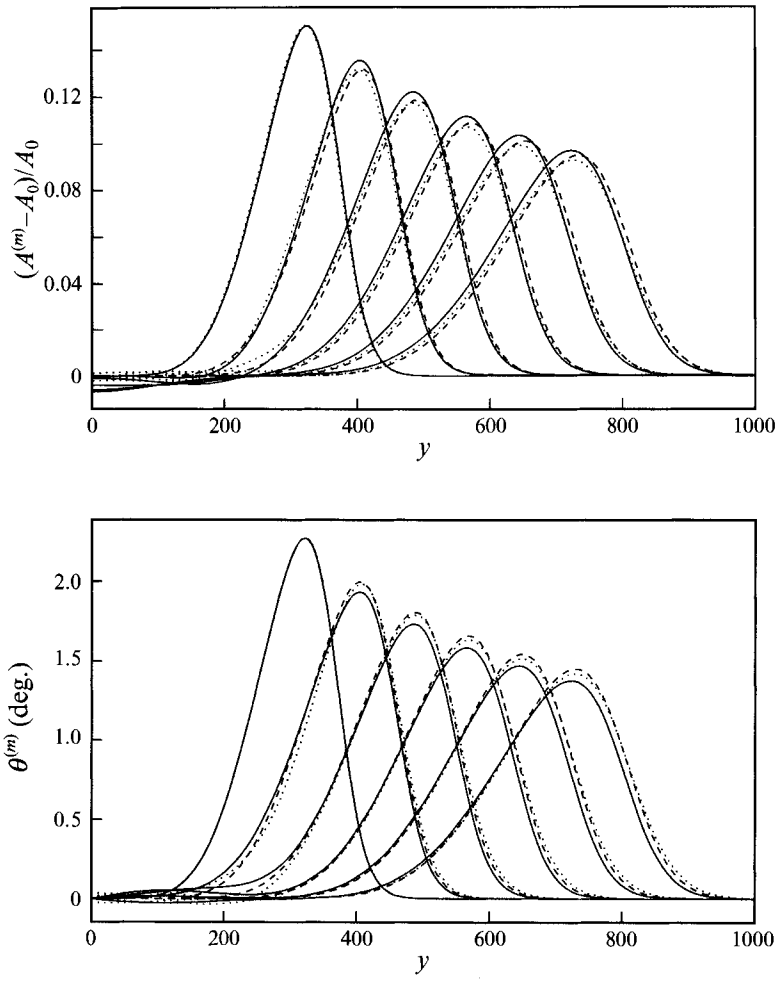

FIGURE 3. Solutions for the same initial conditions and selected times as in figure 2. The numerical solution of the Boussinesq equations is depicted with solid lines, the dashed lines correspond to the Burgers equation (3.25), the dotted line represent the solution of the transport equations (3.20) (3.21) with the leak term intact.

striking. The solution of the simple ray equations steepens and becomes rapidly double-valued even though the initial perturbation is very gentle, whereas the Boussinesq solution instead displays a substantial damping and spreading in line with the time evolution of the self-similar solution (4.2). As shown in figure 3 there is also close quantitative agreement among the solution of the Burgers equation, (4.2), the solution of the Boussinesq equations and the numerical solution of the set (3.20) and (3.21) with the leak term intact. Omitting the last term in (3.20) we observe only very small changes in the solution, θ being altered typically 0.01°. As compared to the higher-order ray solutions the Boussinesq equations yield to high perturbation amplitudes and to small angles. However, the difference evolves mainly during the first part of the simulation, whereas the succeeding trends are quite similar. Thus, the deviations probably stem mainly from the different relations between A and θ that are inherent in the different descriptions of the unidirectional progressive modulations.

In figure 4(a) we have depicted the y-component of the integrated energy flux

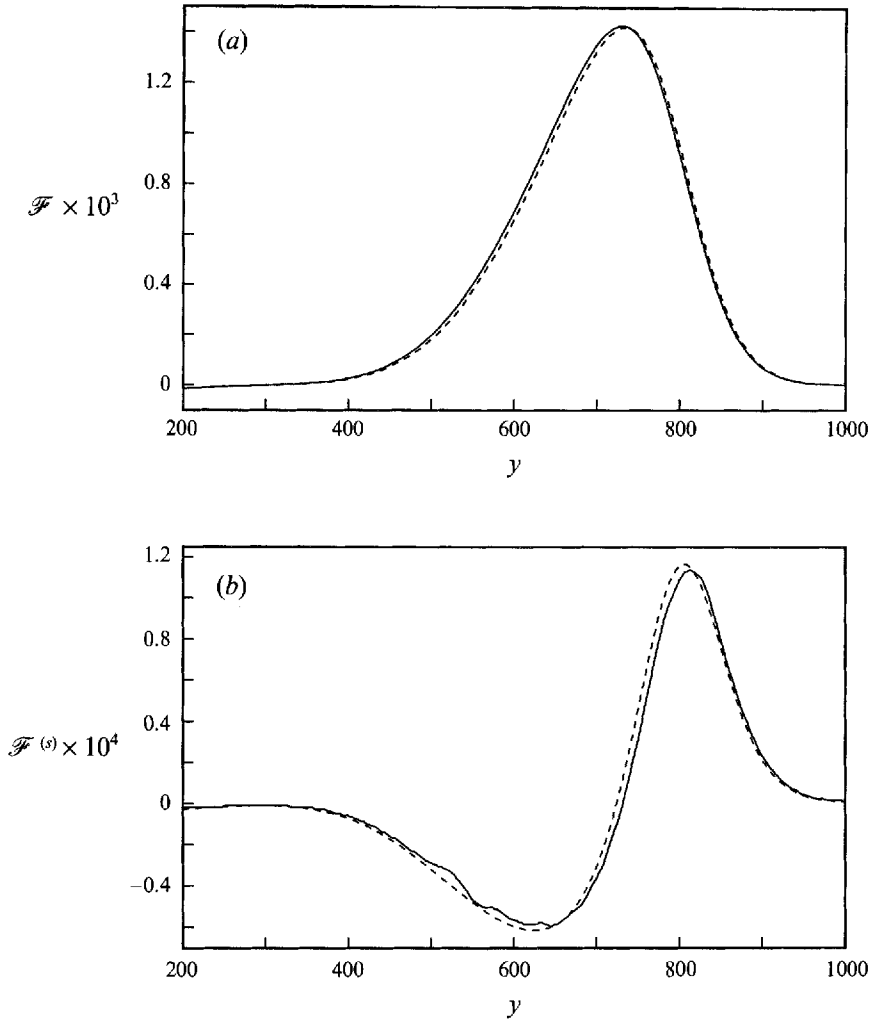

FIGURE 4. Integrated energy fluxes for the case displayed in figure 3 after $t = 2000$. (*a*) The y-component of the flux associated with the leading crest. (*b*) The cross-ray component for the primary crest. Fluxes from the Boussinesq solution are represented by solid lines. The dashed lines correspond to fluxes obtained by substituting the interpolated amplitudes and orientations from this solution into the terms on the right-hand side of (3.16), using the leading approximation for E.

associated with the primary crest, which is the quantity denoted by $\mathscr{F}$ in §3.2. The integration of the numerical solution is performed over the interval $|x - x^{(m)}| < D$ where D is defined according to $Y_0(k_0^{(m)}D) = 10^{-3}$. There is close agreement between (3.16), with the leading representation of E substituted, and the integrated flux from the Boussinesq solution. The cross-ray energy flux component, $\mathscr{F}^{(s)}$, defined as normal to $\boldsymbol{n}^{(m)}(y,t)$ and still integrated within the width of the primary wave, is displayed in figure 4(*b*) together with the last term of (3.16). Again we find convincing agreement, particularly in view of the two levels of interpolation that are involved.

Concerning the higher-order (in β) contributions to the wave field it is very difficult to extract the form correction of the primary wave from the Boussinesq solution owing to its small magnitude compared with discretization and interpolation errors. The cross-ray velocity component, $u^{(s)}$, is on the other hand of order β throughout the

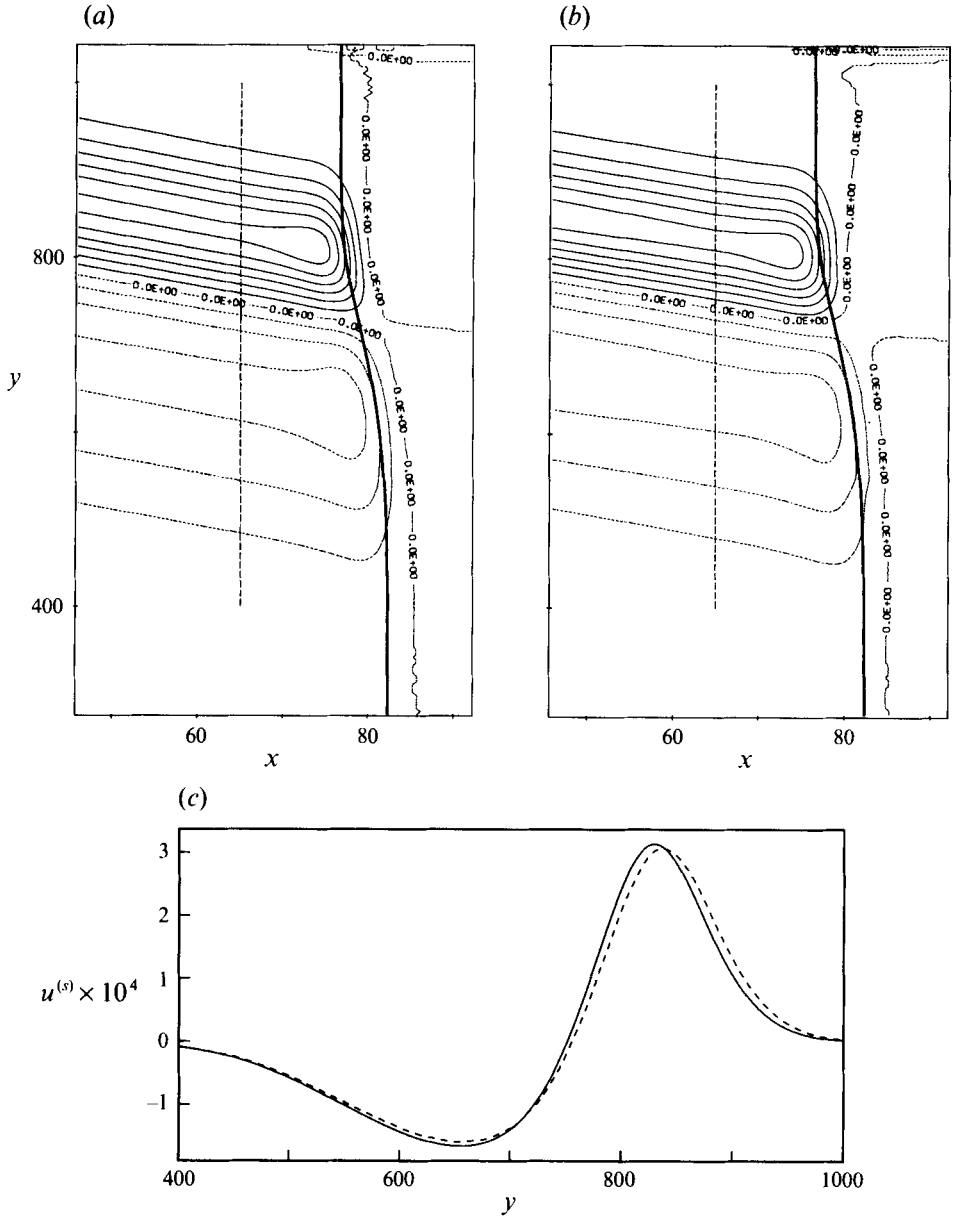

FIGURE 5. Cross-ray velocities for the case displayed in figure 3 after $t = 2000$. (*a*) Contour plot of $u^{(s)}$ obtained from (4.3) and results of §3.3; (*b*) interpolated $u^{(s)}$ from the Boussinesq solution. The contour increment is 0.5×10^{-4}, the relative stretch of the x-scale is 10, the fat solid line shows to the position of the peak and the vertical lines at $x = 65$ correspond to the cross-sections depicted in (*c*). The visible difference in orientation is of order $\tan\theta_d - \theta_d$. (*c*) The velocity u_s at the cross-section $x = 65$. The solid and dashed lines represent the Boussinesq solution and (4.3) respectively.

wave field and can thus be computed also within the primary wave. The definition of cross-ray is still as given above. Employing the solution (3.26) for A and θ we obtain $c_1^{(1)} = 0$ and (3.1) yields

$$u^{(s)} = (B_y \Phi_0 + Bk(\theta - \theta^{(m)})Y_0)(1 + O(\beta, \theta^2, A_0)). \tag{4.3}$$

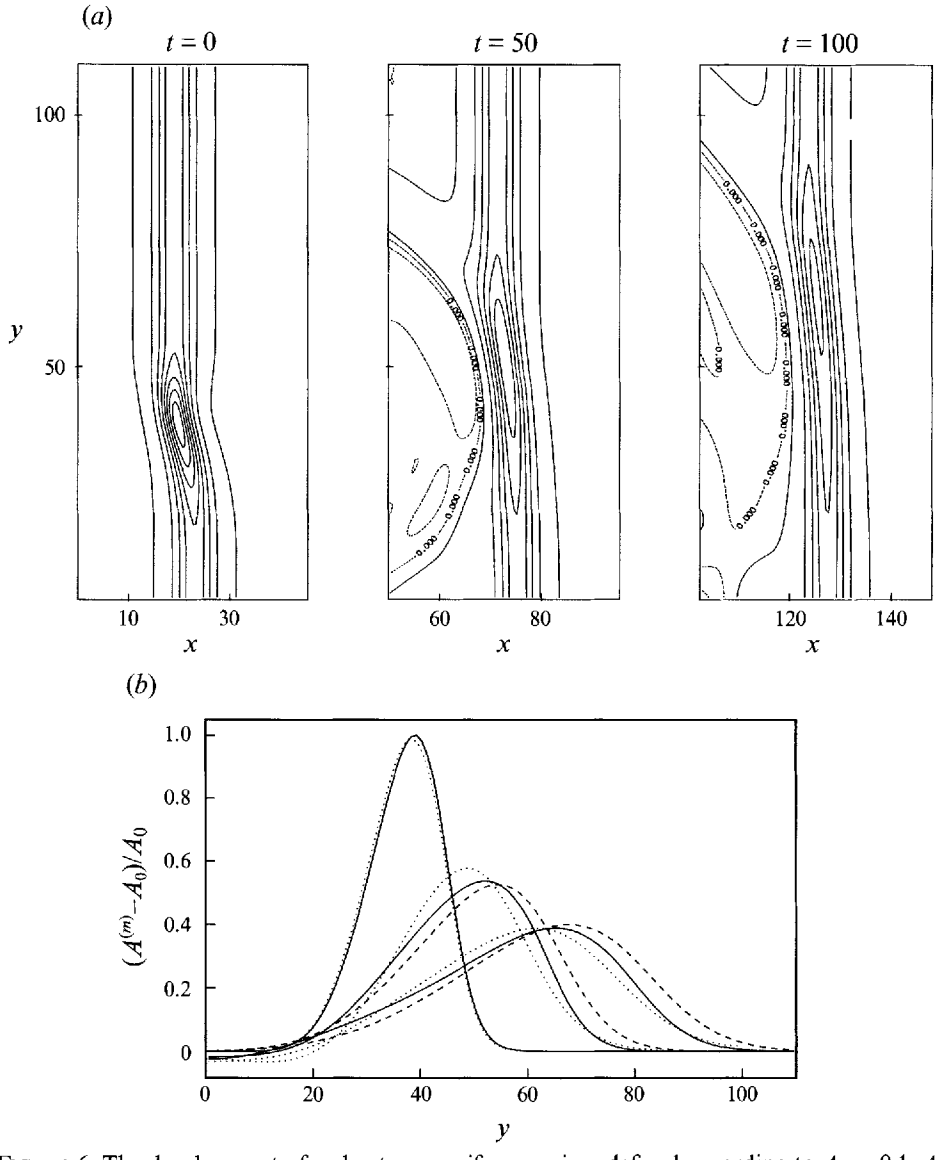

FIGURE 6. The development of a short non-uniform region, defined according to $A_0 = 0.1$, $A_{\max} = 1$ and $L = 8$. (*a*) Contour plot of η obtained by numerical integration of the Boussinesq equations, with 0.025 as contour increment and equally scaled axes. (*b*) Amplitudes calculated by the various equations for $t = 0, 50, 100$. The interpretation of the curve types is as in figure 3 and the discrepancies at $t = 0$ are due to interpolation errors.

We evaluate this expression by extracting $A^{(m)}$ and $\theta^{(m)}$ from the Boussinesq solution and apply the continuation defined through (3.26), (3.8), (3.1) to obtain the complete wave field. As shown in figure 5 the result of this procedure agrees excellently with values directly interpolated from the Boussinesq solution. For the orientation of the diffracted wave field we find $\theta_d \approx 30°$. The deviation from the result $\theta_d = (3A_0)^{\frac{1}{2}} = 31.4°$ of §3.3 is of the same order as in approximations like $\sin\theta_d \approx \theta_d$ that are used frequently throughout the actual calculations.

We will end this subsection by studying the behaviour of a rather abrupt change

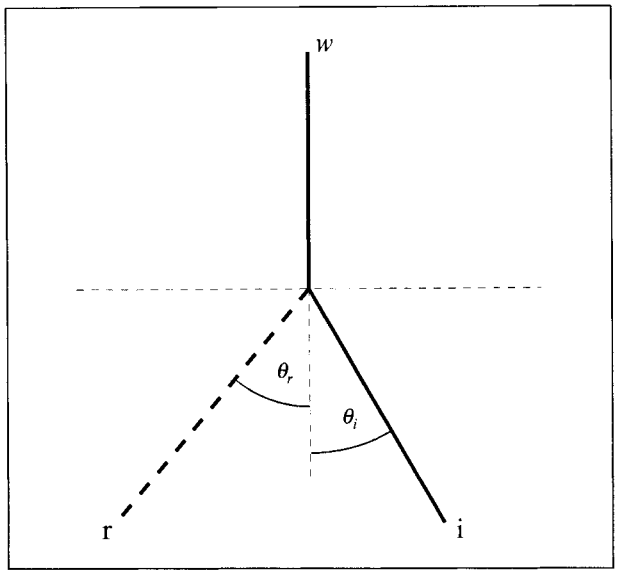

FIGURE 7. A phase-locked triad. The triple point (shock) moves downward and the dashed line depicts the weakest member of the triad. The pattern is oriented like a Mach reflection pattern to make the letters i, r and w denote the incident, stem and reflected waves respectively.

in $x^{(m)}$ corresponding to $A_0 = 0.1$, $L = 8$ and $\Delta_{\max} = 1$. This case must be expected to fall beyond the limits of the ray theory, at least for small t. Still, as shown in figure 6, we observe the same qualitative behaviour as in the previous case with a dominant extension of the transition zone over time. Even the quantitative agreement between the transport equations and the Boussinesq equations is quite good. The diffusion-like spreading is much stronger than for more gentle modulations which suggest that such effects may be more important outside the slowly varying regime than within. This time the diffraction term has a marked influence upon the solution of (3.20) and (3.21) (10% in a), but the picture is by no means dominated by diffraction effects.

4.2. *Wave jumps – comparison to Miles' solution*

According to (3.22) shocks, in the sense of discontinuities of the wave characteristics, will evolve from any initial perturbation of a crest. These are crude representations of wave jumps that often can be initiated by a non-uniform geometry. A familiar example is a vertical wall with a concave corner at which a Mach reflection pattern may start to evolve. Kulikovskii & Reutov (1980) and Liu & Yoon (1986) report wave jumps generated at trenches for solitary and Stokes' waves respectively. The diffusion-like terms of (3.21), (3.20) or (3.25) must be expected to inhibit development of discontinuities and instead enable a more detailed description of jumps of finite width.

A complete discussion of a jump, in the sense of an relative abrupt change in amplitude and orientation of the carrier wave, is found in Miles (1977*b*) which is the second paper of a pair (Miles 1977*a*, *b*) presenting an excellent analysis of obliquely interacting solitons. In that context the shock is described as a phase-locked triad for which analytical solutions are presented. These solutions are accurate to the same order as the Boussinesq equations. A definition sketch of such a triad is shown in figure 7. The pattern is completely determined by the amplitude at one side of the shock and the jump in orientation, corresponding to θ_i. Using the conventions implicit

in the figure, we may write the asymptotic relations of Miles' solution as

$$\left.\begin{aligned} \theta_r &= (3A_i)^{\frac{1}{2}}, \qquad A_w = A_i(1+\theta_i/\theta_r)^2, \\ A_r &= \tfrac{1}{3}\theta_i^2, \qquad\quad U_m = \left(\tfrac{1}{3}A_i\right)^{\frac{1}{2}}(1-\theta_i/\theta_r), \end{aligned}\right\} \tag{4.4}$$

where U_m is the speed of the triple point, A_i and A_w are the amplitudes ahead and behind of the jump respectively, while A_r and θ_r define the characteristics of the third wave. In the present context this wave may be regarded as a diffraction from the jump zone that is not inherent in the lowest-order (pure hyperbolic) ray theory. After being rescaled according to (2.1) the surface elevation from Miles' solution reads

$$\tfrac{1}{4}\eta = \frac{A_i e^{4\chi_w - 2\chi_i} + A_w e^{2\chi_w} + A_r e^{2\chi_r}}{(1+e^{2\chi_w}+e^{2\chi_r})^2}, \tag{4.5}$$

where the phases are given according to

$$\chi_i = \frac{(3A_i)^{\frac{1}{2}}}{2}(\cos\theta_i(x-x_f)+\sin\theta_i(y-y_f)), \quad \chi_w = \frac{(3A_w)^{\frac{1}{2}}}{2}(x-x_f), \quad \chi_r = \chi_w - \chi_i, \tag{4.6}$$

and the values of x_f and y_f determine the location of the triple point. It is easily deduced that the shock width is proportional to θ_i^{-1}. Thus, provided $A_i^{-\frac{1}{2}}\theta_i \ll 1$ the Burger equation (3.25) should reproduce the above jump relations to leading order. First we note that the angle θ_r from (4.4) is identical to the general angle of diffracted wave systems that was found in §3.3. Next, finding a permanent-form jump solution of (3.25) and re-inserting the scaling (2.1) we obtain

$$A = A_i\left(1+\frac{\theta_i}{(3A_i)^{\frac{1}{2}}}\left(1+\tanh\left(\frac{(3A_i)^{\frac{1}{2}}}{2}\theta_i(y+U_m t)\right)\right)\right), \tag{4.7}$$

where the shock speed U_m is as given in (4.4). However, the shock speed depends solely on the asymptotic characteristics of the jump (A_i, A_w and θ_i) and is not affected by the diffusion-like terms of the corrected ray theory. The jump profile, on the other hand, is crucially dependent on these terms and does coincide with Miles' solution in the limit $A_i^{-\frac{1}{2}}\theta_i \to 0$, $A_i \to 0$. This is most easily demonstrated through calculation of the diffracted wave (3.11), (3.26) that to leading order becomes a soliton with amplitude equal to A_r as given in (4.4). The asymptotic agreement with Miles' solution clearly demonstrates the validity of the present theory.

In figure 8 we have displayed $A^{(m)}$ for two jumps, corresponding to $A_i = 0.05$, $\theta_i = 0.5°$ and $A_i = 0.02$, $\theta_i = 7°$ respectively. Whereas the first case yields a very large jump width, the validity of the ray description is more questionable for the latter. However, even for the second case we obtain rather good results from the transport equations (3.20) and (3.21).

4.3. *Axisymmetric converging waves*

Propagation and evolution of axisymmetric waves in the weakly nonlinear and dispersive regime have been the subjects of several papers, for example Cumberbach (1978) and Miles (1977*d*). Ko & Kuehl (1979) reported a perturbation technique closely related to the present one. They found good agreement between their analytical results and numerical simulations concerning the amplification of focusing cylindrical and spherical waves. However, no detailed comparison for the wave profiles was presented.

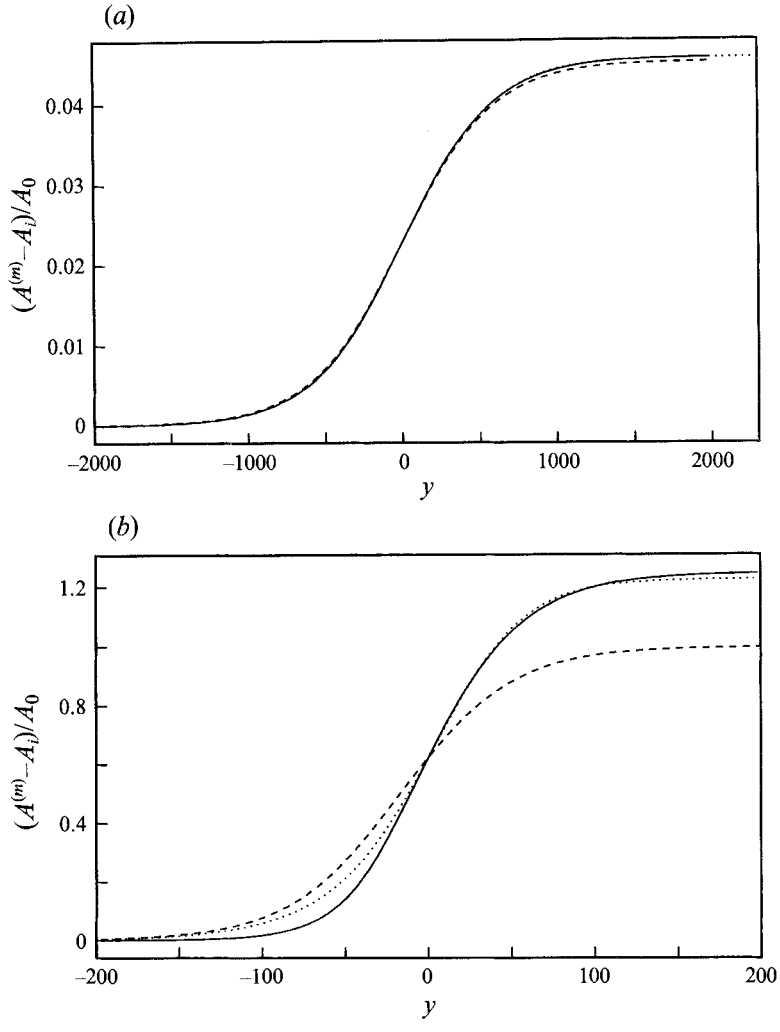

FIGURE 8. The variation of the amplitude, $A^{(m)}$, across wave jumps. (*a*) $A_i = 0.05$ and $\theta_i = 0.5°$, (*b*) $A_i = 0.02$ and $\theta_i = 7°$. The jump solution of Miles is depicted with solid lines, the dashed lines correspond to the Burgers equation (3.25) and the dotted lines represent the solution of the transport equations (3.20) (3.21) with the leak term intact. We have chosen the position where Miles' solution predicts $A^{(m)} = \frac{1}{2}(A_i + A_w)$ as origin.

The main objective of the present study of focusing waves is to seek direct verification of the representations of $\hat{\eta}$ and $c_1^{(0)}$ in §3 through comparison to accurate numerical solutions of the Boussinesq equations. The variable coefficients of the cylindrical Boussinesq equations introduce no difficulties concerning numerical solution, apart from the extra caution required to resolve the neighbourhood of $r = 0$. We apply a straightforward adaptation of the method in Pedersen (1988) and any further description should be superfluous. For each numerical calculation the discretization errors are estimated by grid refinement tests. Values for the height, $\eta_{\max}$, and position, $r_{\max}$, of the crest peak are generally improved through a simple extrapolation routine that utilizes the second-order (in grid increments) convergence of the numerical method.

To the significant order (3.8) gives the following relation between $r_{\max}$, $\eta_{\max}$ and

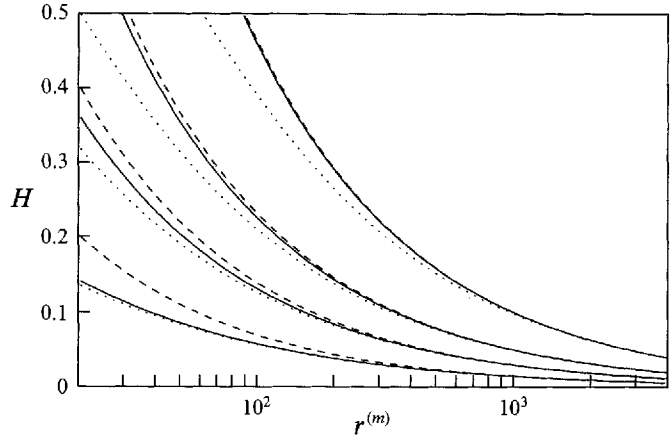

FIGURE 9. Height of the primary wave, $H = A^{(m)}Y(0, A^{(m)})$ versus $r^{(m)}$ for different approximations to (3.27) as explained in the text: ——, (i); - - - -, (ii); · · · ·, (iii).

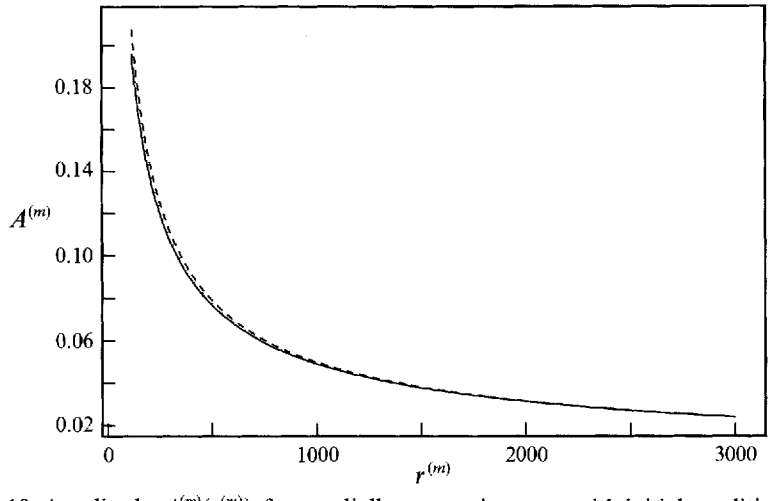

FIGURE 10. Amplitude, $A^{(m)}(r^{(m)})$, for a radially converging wave with initial conditions corresponding to a plane soliton solution with parameters $r_0 = 4000$, $H_0 = 0.0198$. We have depicted the numerically calculated amplitude (——), the amplitude from (3.27) without the leak term (- - - -) and the amplitude predicted by the complete equation (3.27) (· · · ·). The energy equation (3.27) is applied with the modified reference point $r_0 = 2999.8$, $A_0 = 0.0239$ to avoid the effect of inaccurate initial conditions.

$A^{(m)}$, $r^{(m)}$:

$$\eta_{\max} = H + \frac{2}{3r^{(m)}(3A^{(m)})^{\frac{1}{2}}}, \quad r_{\max} = r^{(m)} + \frac{2}{3r^{(m)}(A^{(m)})^2}, \tag{4.8}$$

where the height of the primary wave is given as $H = A^{(m)}Y(0, A^{(m)})$. When $\eta_{\max}$ and $r_{\max}$ are found from the numerical solution the above equations can be inverted to yield $A^{(m)}$ and $r^{(m)}$, whereafter the whole perturbation solution can be calculated at the given instant. In the comparisons that are to follow we use exact representations, belonging to the Boussinesq equations, for Y and c_0 as functions of H.

The significance of the diffraction is illustrated in figure 9 where we have depicted

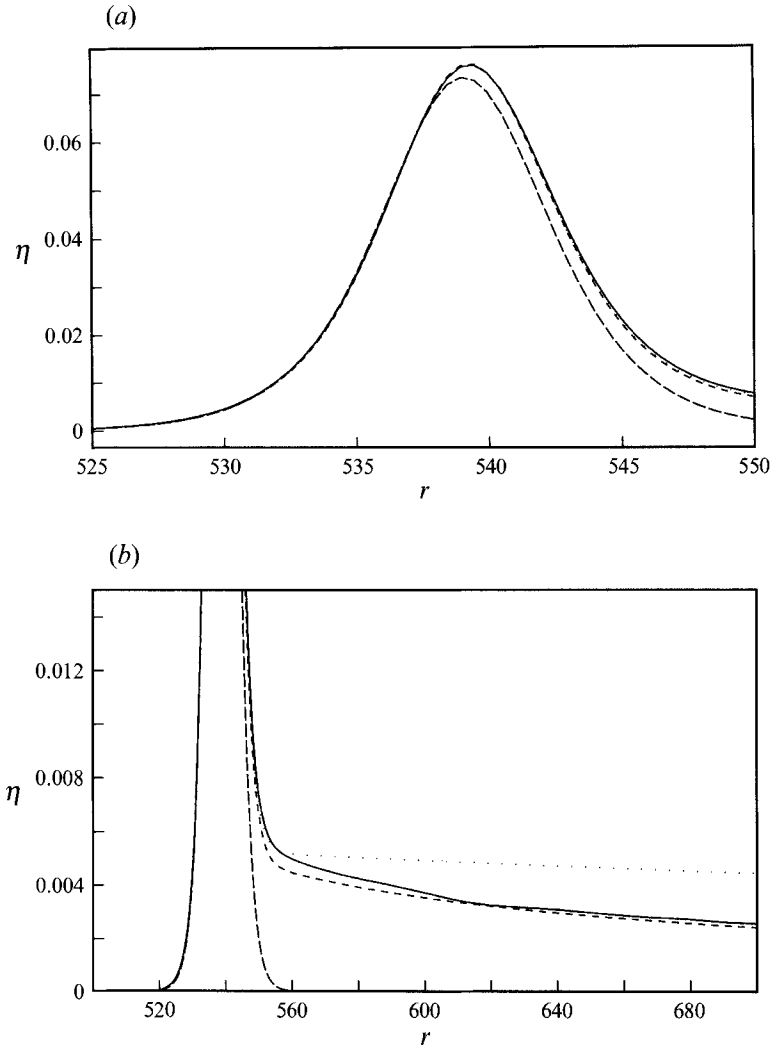

FIGURE 11. The surface elevation at $t = 3400$ for a radially converging wave with initial conditions corresponding to a plane soliton solution with parameters $r_0 = 4000$, $A_0 = 0.0198$. We have depicted the numerically calculated surface elevation (——), the unified perturbation solution (- - - -) defined by (3.28), the soliton profile (– – –) and the local perturbation solution (· · · ·) defined by $A = A^{(m)}$. The last three curves are based on the location and size of the maximum surface elevation in the numerical Boussinesq solution.

results from (3.27). Wave heights of the primary crest are displayed for three different levels of approximation:

(i) We retain the diffraction term, approximate E by $8 \times 3^{-\frac{3}{2}}(A^{(m)})^{\frac{3}{2}}$ and put $H = A^{(m)}$, corresponding to the approximation $Y \approx Y_0$.

(ii) As (i), except that the logarithmic diffraction term is omitted.

(iii) The diffraction term is retained and we have invoked the second-order representations for E and Y as given in (2.5).

In the figure we have depicted the $H(r^{(m)})$ curves for the reference position $r_0 = 1000$ and the reference wave heights $H_0 = 0.1, 0.05, 0.03, 0.015$. It is apparent that the energy leak dominates higher-order contributions to E and Y only for the case corresponding

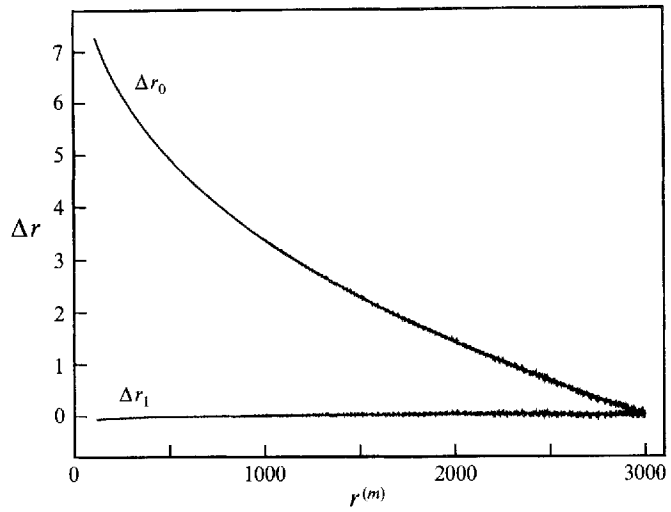

FIGURE 12. Errors for zeroth- and first-order approximation, in terms of β, to $r^{(m)}$ as given in (4.9). The flossy appearance of the curves is probably due to interpolation errors.

to the smallest reference wave height. Regarding comparison to numerical solutions of the Boussinesq equations we may thus expect improved agreement due to the diffraction term in (3.27) only for the domain in the $(H, r^{(m)})$-plane close to or below the lowest curve in the figure. We also see that the leading representation of E yields good results for $A < 0.25$, say.

In figure 10 we have compared the amplification in a numerical simulation to the predictions of (3.27) corresponding to (i) and (ii) above. The numerical integration was initiated with $H_0 = 0.0198$, $r_{\max} = 4000$ and initial conditions corresponding to the exact plane soliton solution of the Boussinesq equations. However, the comparison is started when $r_{\max} < 3000$ and the wave pattern presumably has been nearly fully developed. The agreement is as least as good as can be expected in view of the results in figure 9. According to the same figure we should not over-emphasize the improved agreement due to the leak term for this case. Wave profiles for $t = 3400$ are compared in figure 11. We observe that the contribution from $\hat{\eta}$ is significant and that the profile belonging to (3.28) agrees well with the numerical solution for the crest as well as the diffracted tail. The most pronounced deviations are found at the head of the tail where the numerical solution displays some weak undulating behaviour. This feature resemble the tail generated when a plane soliton evolves from a slightly perturbed initial condition and is significantly altered neither by invoking the full perturbation solution as initial conditions, starting the soliton from a larger $r_{\max}$ nor by refining the grid. We are thus led to suggest that undulations reflect the 'struggle' of the primary wave to preserve its identity and solitary shape. It is not investigated to what extent these effects may be included through higher-order terms of the perturbation expansion. Assuming a spatially constant A we find equally good agreement for the leading crest as for (3.28), but the tail is not reproduced.

Whereas the factor $c_1^{(0)}$ was essential for the appropriate description of wave jumps in the preceding section, it is of minor importance in the context of axisymmetric waves. On the other hand, numerical solutions for radially converging waves provide an excellent opportunity for direct validation of the expression (3.7). Given $H(t)$ and $r^{(m)}(t)$, as extracted from the numerical solution, we may calculate the inherent errors

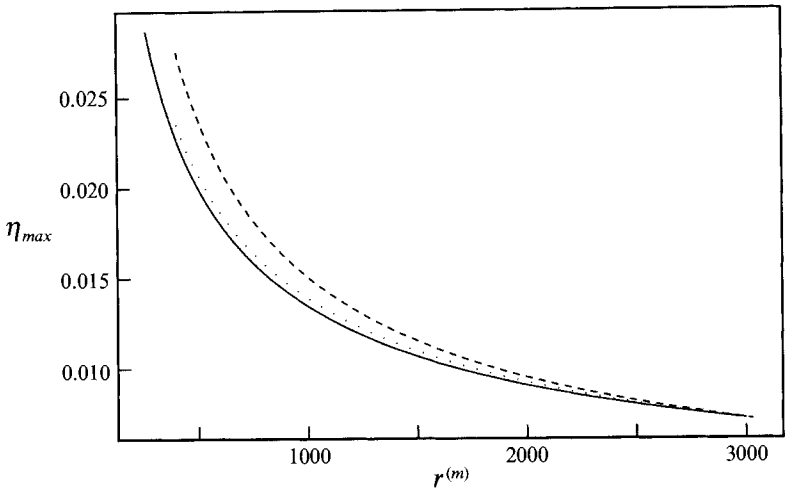

FIGURE 13. The total wave height $\eta_{\max}$ for a radially converging wave with initial conditions corresponding to a plane soliton solution with parameters $r_0 = 6000$, $\eta_{\max} = 0.005$. We have depicted the amplitude calculated numerically (——), the amplitude from (3.27) without the leak term (- - - -) and the amplitude predicted by the complete equation (3.27) (· · · ·). The energy equation (3.27) is applied with the modified reference point $r_0 = 2999.0$, $\eta_{\max} = 0.00723$ to reduce the effect of inaccurate initial conditions.

in two anticipated positions according to

$$\Delta r_0 = r^{(m)}(t_1) - \int_{t_1}^{t} c_0(H)\mathrm{d}t - r^{(m)}, \quad \Delta r_1 = \Delta r_0 - \int_{t_1}^{t} \frac{c_0}{r^{(m)}(3H)^{\frac{1}{2}}}\mathrm{d}t, \tag{4.9}$$

where c_0 is the exact soliton speed belonging to the Boussinesq equations and the second integrand is recognized as $c_1^{(0)}$ for the radially symmetric case. For the same case as above we have displayed the two dislocations in figure 12. It is apparent that the retention of $c_1^{(0)}$ reduces the error by an order of magnitude.

Finally, in figure 13, we have depicted the amplification of a wave with initial parameters $r_0 = 6000$, $\eta_{\max} = 0.005$ that roughly correspond to the lowest curve in figure 9. We observe that the presence of the leak term improves the agreement with the numerical solution markedly. However, it must be noted that the displayed case probably is at the limit on the validity range of the perturbation solution.

5. Concluding remarks

Numerical solutions of the Boussinesq equations confirm the existence of progressive modulations on a solitary-wave-like crest as predicted by standard ray theory. However, the full Boussinesq solutions inherit a pronounced damping of the modulation – a feature that cannot be reproduced by the purely hyperbolic ray equations reported previously. Corrections to the primary wave field are obtained by a two-scale perturbation technique that also yields a formal derivation of the first-order ray equations. In two special cases, infinitesimal modulations on a straight crest and axisymmetric focusing, we find uniform solutions of very compact form for the secondary wave field. However, an explicit calculation of the diffracted field is not required for the development of a corrected ray theory. Incorporating the secondary wave field in an energy balance argument for the head wave we obtain a second-order

transport equation that possess principally new features. One is the cross-ray energy transport due to lateral velocities. Equally important is the dependence of both integrated energy density and overall wave celerity speed on the curvature of the primary crest. An energy sink, due to the diffracted waves, does also appear, but proves to be less important for the presented examples.

The new terms of the amended ray theory turn the transport equations into a mixed hyperbolic/parabolic form. Consequently the progressive modulations are damped and we observe excellent agreement with the Boussinesq equations. Also the integrated energy fluxes, cross-ray velocity components and diffracted wave field approximate closely the corresponding quantities of the full solution. Very strong diffusion-like damping and spreading are recognized in the numerical simulation of initially short modulations on the principal crest. Even in this case we obtain quantitatively good results from our higher-order ray theory.

The application of ray theory to fully developed wave jumps is primarily limited to weak shocks and small amplitudes. For such shocks the amended transport equations predict a finite width and, together with the detailed perturbation solution, also a diffracted wave originating from the jump zone. In the limit of weak shocks this description is found to be perfectly consistent with Miles' solution for a resonant triad of solitons, with the diffracted wave as the third member. The proper reproduction of weak wave jumps is a convincing proof of the validity of the presented theory. Again we obtain quantitatively good predictions from the ray theory for short crest transition also, this time in the form of a strong jump.

For axisymmetric waves our perturbation solution, although developed in a different form and organization, can be shown to be fully consistent with the results of Ko & Kuehl (1979). The new terms in the transport equations are much less important for radially converging waves. Naturally, there is no cross-ray energy transport in this case. In addition, the leading contribution from the curvature-dependent part of the energy density integrates to a constant in the final energy equation. However, we obtain very good agreement with accurate numerical simulations concerning both the detailed wave profiles and the curvature-dependent correction to the propagation speed, thereby establishing further confirmation of the perturbation solution.

We conclude that higher-order effects in ray theory may often be important for the qualitative behaviour of modulated solitary waves. A similar importance of the diffusion-like effects must be expected also for other single-crested 'hump shaped' waves. Waves of essentially sinusoidal shape are, on the other hand, probably much less influenced since the cross-ray energy transport etc. is likely to cancel over an period.

Appendix A. The perturbation expansion

The local wavenumber and phase speed, defined by (3.2), have to fulfil the consistency relations

$$\boldsymbol{k}_t + \nabla(kc) = 0, \quad \nabla \times \boldsymbol{k} = 0. \tag{A 1}$$

Owing to nonlinear interaction between the primary and secondary wave field we expand c and $\boldsymbol{k}$ according to

$$c = c_0 + \beta c_1, \quad \boldsymbol{k} = \boldsymbol{k}_0 + \beta \boldsymbol{k}_1, \tag{A 2}$$

where c_0, k_0 relate to A as described in (2.5) and c_1, $\boldsymbol{k}_1$ are functions of χ and the slow variables. Using the definitions below (3.4) we decompose the wavenumber correction

according to $\boldsymbol{k}_1 = N\boldsymbol{n} + S\boldsymbol{s}$. Exploiting (A 1) we find that N drops out to order β whereas c_1 and S are at most linear functions of χ as indicated in (3.3) and (3.4). Since both c_0 and $c_1^{(1)}$ inherit only slow variation the term βc_1 may become comparable with c_0 for large χ, thereby violating the uniformity of the expansion (A 2). This indicates that only local validity of the perturbation solution can be anticipated when $c_1^{(1)}$ is non-zero. On the other hand, the fast variation associated with χ must be expected to vanish exponentially when $|\chi| \to \infty$. It turns out that we generally obtain a solution that is local in the slow variables, but still correct for large χ. We are now led to the kinematic relations

$$k_{0,\hat{t}} + c_f k_{0,\hat{n}} = -k_0^2 c_1^{(1)} + O(\beta), \tag{A 3}$$

$$\theta_{\hat{t}} + c_f \theta_{\hat{n}} = (c_0 - c_f) S^{(1)} + O(\beta). \tag{A 4}$$

The factor $c_f = \mathrm{d}(k_0 c_0)/\mathrm{d}k_0 = 1 + \frac{3}{2}A + O(A^2)$ bears a formal resemblance to the group velocity for sinusoidal waves and occurs in a similar fashion as far as the kinematic equations are concerned. It will be shown below that these two equations must be supplemented by a third equation, (3.5), that emerges from the solubility condition for $\hat{\eta}$ and $\hat{\phi}$. If $c_1^{(1)}$ and $S^{(1)}$ were not included in the calculation, we would then have a set of three equations for the two unknowns A and θ, for which the existence of a solution is far from obvious beforehand. The retention of $c_1^{(1)}$ and $S^{(1)}$ does also reconcile the present approach to those reported previously. The calculations of Grimshaw (1970, 1971) and Ko & Kuehl (1978, 1979) were based on a phase function that is slightly different from the one used herein. Denoting their phase function by $\hat{\chi}$ we may write $\chi = p(\hat{x}, \hat{y}, \hat{t})\hat{\chi}$. Defining the corresponding phase velocity by $\hat{c} \equiv -\hat{\chi}_{\hat{t}}/\hat{\chi}_{\hat{x}}$ we then deduce

$$c \equiv -\chi_t/\chi_x = \hat{c} - \frac{\beta}{pk}(p_{\hat{t}} + \hat{c}p_{\hat{n}})\chi + O(\beta^2), \tag{A 5}$$

which is clearly consistent with (3.3).

At the peak of the primary wave only $c_1^{(0)}$ will contribute to the wave celerity. As an alternative to the introduction of $c_1^{(0)}$ we could have allowed A to be redefined to each order in β. To avoid ambiguity we must exclude such modifications that, according to (2.5), will appear as

$$\hat{\eta} = \ldots + A_1(\hat{x}, \hat{y}, \hat{t})(Y_0 + \tfrac{1}{2}\chi Y_{0,\chi}) + \ldots, \tag{A 6}$$

where βA_1 is the first-order amplitude correction. We are also left with some freedom concerning the spatial variation in A in relation to the factors $c_1^{(1)}$ and $S_1^{(1)}$. Apart from plane and axisymmetric cases a lateral (along primary crest) variation in A must be fully included. The normal variation, however, is less essential and may, in analogy with (A 6), be replaced by a contribution to the secondary wave field of the form

$$\hat{\eta} = \ldots + \frac{A_{\hat{n}}^{(m)}}{k^{(m)}}(\chi Y_0 + \tfrac{1}{4}\chi^2 Y_{0,\chi}) + \ldots. \tag{A 7}$$

Contrary to that in (A 6) this term will have no implications for the derivation of the higher-order transport equations in §3.2 because it is odd in χ.

Generally we must expect that a residual system of diffracted waves is trailing the leading crest. Thus, we may impose that $\hat{\eta}$ and $\hat{\phi}$ vanish asymptotically upstream ($\chi \to \infty$), while allowing an infinite extension downstream for the first-order wave field. Inserting (3.1), (3.2) and (A 2) into (2.2) and (2.3) and integrating the continuity equation with respect to χ we find that the leading balance is automatically fulfilled

through the definition of the soliton solution, while to first order in β we obtain

$$-c_0\hat{\eta} + k_0\hat{\phi}_\chi = c_1^{(0)}AY + c_1^{(1)}A\int_\infty^\chi \chi Y_\chi \mathrm{d}\chi$$

$$-k_0^{-1}A_{\hat{t}}\int_\infty^\chi Y\,\mathrm{d}\chi - k_0^{-1}(2\hat{\nabla}B\cdot\boldsymbol{k}_0 + B\hat{\nabla}\cdot\boldsymbol{k}_0)\Phi + S_1, \tag{A 8}$$

$$-\hat{\eta} + c_0k_0\hat{\phi}_\chi = -(c_1^{(0)} + c_1^{(1)}\chi)k_0B\Phi_\chi + B_{\hat{t}}\Phi + S_2, \tag{A 9}$$

where $S_1, S_2 = O(A^{\frac{3}{2}})$. The set (A 8) and (A 9) can be ruled by two alternative dominant balances, corresponding to different representations of the secondary wave field. In any case it turns out that

$$\hat{\eta} = O(A^{\frac{1}{2}}), \quad \theta_{\hat{s}} = O(A), \quad c_1^{(0)}, c_1^{(1)} = O(A^{\frac{1}{2}}). \tag{A 10}$$

We may summarize the two choices as follows:

(i) $-\hat{\eta} + k_0\hat{\phi}_\chi = O(A^{\frac{1}{2}})$.

A solution for $\hat{\eta}$ and $\hat{\phi}$ is now possible only if

$$A_{\hat{t}},\, A_{\hat{n}} = O(A); \quad T \equiv B_{\hat{t}} + k_0^{-1}(A_{\hat{t}} + 2\hat{\nabla}B\cdot\boldsymbol{k}_0 + B\hat{\nabla}\cdot\boldsymbol{k}_0) = O(A^{\frac{3}{2}}). \tag{A 11}$$

To leading order (A 3) now implies $A_{\hat{t}} + A_{\hat{n}} = O(A^2)$ which is consistent with (A 11). In this case all $O(A^{\frac{3}{2}})$ terms in S_1, S_2 become significant. Consequently, the higher-order terms in (2.5) will enter the calculations. However, a careful consideration involving higher-order long-wave equations shows that the perturbation still can be appropriately performed starting from (2.2) and (2.3).

(ii) $-\hat{\eta} + k_0\hat{\phi}_\chi = O(A^{\frac{3}{2}})$.

As compared to the preceding option the variation of A becomes one order higher in A, according to $A_{\hat{t}}$, $A_{\hat{n}} = O(A^2)$. Consequently, the variation of A and k_0 cannot contain the $O(\beta)$ modifications of the wave profile and a term like (A 7) is bound to appear. The solution for $\hat{\eta}$ and $\hat{\phi}$ is again determined through the $O(A^{\frac{3}{2}})$ balance of (A 8) and (A 9). However, this time we may retain only the terms in S_1 and S_2 that contain $\hat{\eta}$ or $\hat{\phi}$.

Only the balance (i) enables compact and uniform solutions, while (ii) yields much simpler calculations. For the derivations below we assume behaviour (i). The alternative choice would involve the same main steps and lead to equivalent final equations (3.5)–(3.9). Some of the terms that are retained in these equation would, however, become insignificant.

Eliminating $\hat{\phi}$ we find a linear second-order equation for $\hat{\eta}$ that is readily solved:

$$\hat{\eta} = D_1(\hat{x},\hat{y},\hat{t})Y_{0,\chi} + D_2(\hat{x},\hat{y},\hat{t})G(\chi) - (\tfrac{1}{2}(3A)^{-\frac{1}{2}}A_{\hat{t}} - A^{-1}T - c_1^{(1)})\Phi_0$$

$$+(2c_1^{(0)} - 3(\tfrac{1}{2}(3A)^{-\frac{1}{2}}A_{\hat{t}} - A^{-1}T - c_1^{(1)}))(Y_0 + \tfrac{1}{2}\chi Y_{0,\chi})$$

$$+\tfrac{5}{4}(\tfrac{1}{2}(3A)^{-\frac{1}{2}}A_{\hat{t}} + A^{-1}T)R(\chi) + 2c_1^{(1)}(\chi Y_0 + \tfrac{1}{4}\chi^2 Y_{0,\chi}) + O(A^{\frac{3}{2}}), \tag{A 12}$$

where Φ_0 is as defined below (3.9), D_1 and D_2 are constants of integration and $G \sim \exp|\chi|$, $R \sim \exp 2|\chi|$ as $|\chi| \to \infty$. Hence, D_2 as well as the coefficient before R in (A 12) have to be zero, which imply (3.5). According to the discussion below (A 2) we must also discard the term on the second line of (A 12), thereby assigning a

value to $c_1^{(0)}$. Generally, any terms involving powers of χ, instead of neatly behaved combinations of exponentials, look suspicious and should preferably be reinterpreted or removed by an improved construction of the perturbation scheme. Also the last term of (A 12) contains potential factors of χ. However, this term, which is of the form given in (A 7), can be removed only by finding solutions for A and θ giving zero $c_1^{(1)}$. Now, the term $D_1 Y_{0,\chi}$ is easily seen to correspond to a non-uniform representation of a redefined phase function given by $\chi \to \chi + \beta D_1$. This redefinition will not alter the profile of the principal crest to order β and corresponds to $O(\beta^2)$ modifications in $\boldsymbol{k}$ and c that preferably should enter the solution through higher-order corrections to the transport equations. The fact that Ko & Kuehl find a distinct value for D_1 from a higher-order solubility condition is probably due to the absence of expansions, like (A 2), for c and k in their perturbation scheme. Clearly, in a consistent and compact expansion we can put D_1 to zero. In addition we may note that this term will not contribute anyway to the energy integrals in §3.2. Using the dominant balance inherent in the kinematic equations (A 3) and (A 4) the above results are summarized to give (3.5)–(3.9).

Appendix B. Numerical solution of the ray equations

Following Pedersen (1988) we use the notations δ_q and $\overline{()}^q$ for the divided midpoint difference and average with respect to the variable q. These operators involve two neighbouring points and give discrete approximations to the first-order partial derivative and the function itself, respectively. The grid site of a quantity is denoted by a subscript for the spatial location and a superscript for the time. We further collect terms within square brackets, while leaving common indices outside.

Both the kinematic equation, (3.21), and the energy equation, (3.20), are written in a conservative form and display a mixed hyperbolic/parabolic nature. Using $e \equiv (A^{(m)})^{\frac{3}{2}}$ as a new dependent variable we may write

$$\frac{\partial e}{\partial t} = -\frac{\partial B}{\partial y} - D, \quad \frac{\partial \theta}{\partial t} = -\frac{\partial G}{\partial y}, \tag{B 1}$$

for the energy and kinematic equations respectively. The symbol D denotes the energy sink, while B and G are transport terms. Thus, apart from some of the nonlinearities and the interpretations of the unknowns, the set is of a standard type described in an array of textbooks. Consequently, there should be need for no more than a brief documentation on the numerical method.

Contrary to the most standard textbook procedures we apply a staggered grid both in time and space and choose $e_j^{(n+\frac{1}{2})}$ and $\theta_{j+\frac{1}{2}}^{(n)}$ as unknowns. The difference equations read

$$[\delta_t e = -\delta_y B - D]_j^{(n)}, \quad [\delta_t \theta = -\delta_y G]_{j+\frac{1}{2}}^{(n+\frac{1}{2})}, \tag{B 2), (B 3}$$

where the fluxes are represented according to

$$[B = \theta \tilde{e} - 3^{-\frac{3}{2}} (\overline{e^{y}}^{t})^{-\frac{1}{3}} \delta_y \overline{e}^{t}]_{j+\frac{1}{2}}^{(n)} \tag{B 4}$$

$$G_j^{(n+\frac{1}{2})} = [\tfrac{1}{2} e^{\frac{2}{3}} - 3^{-\frac{1}{2}} e^{-\frac{1}{3}} \delta_y \overline{\theta}^{t}]_j^{(n+\frac{1}{2})} + \tfrac{1}{2} \tilde{\theta}_j^{(n+1)} \tilde{\theta}_j^{(n)}. \tag{B 5}$$

The meaning of the tilde depends on whether we use an up-wind scheme or not. If a symmetric scheme is used, the tilde simply denotes the midpoint average as defined in the introduction to this Appendix. On the other hand, when we use up-wind

differences in the advection terms, the tilde indicates the nearest upstream value ($\tilde{e}_{j+\frac{1}{2}} = e_j$ if $\theta_{j+\frac{1}{2}} > 0$ etc.). Upstream representations have to be used whenever the diffusion-like terms on the right-hand sides of (3.20) and (3.21) become very small. However, most of simulations described herein are performed with symmetric differences. The energy sink term is discretized according to

$$[D = 3^{-\frac{3}{2}} \left(\delta_y \theta\right)^2 + 3^{\frac{1}{2}} \left(\delta_y (\bar{e}^{yt})^{\frac{1}{3}}\right)^2]^{(n)}_{j+\frac{1}{2}} . \tag{B 6}$$

At each time level the equations (B 2) and (B 2) give implicit equations for new e- and θ-values respectively. The former is nonlinear and is solved by an iteration technique.

REFERENCES

CUMBERBACH, E. 1978 Spike solution for radially symmetric solitary waves. *Phys. Fluids* **21**, 374–380.

GRIMSHAW, R. 1970 The solitary wave in water of variable depth. *J. Fluid Mech.* **42**, 639–656.

GRIMSHAW, R. 1971 The solitary wave in water of variable depth. Part 2. *J. Fluid Mech.* **46**, 611–622.

KO, K. & KUEHL, H. H. 1978 Korteweg-de Vries soliton in a slowly varying medium. *Phys. Rev. Lett.* **40**, 233–236

KO, K. & KUEHL, H. H. 1979 Cylindrical and spherical Korteweg-deVries solitary waves. *Phys. Fluids* **22**, 1343–1348

KULIKOVSKII, A. G. & REUTOV, V. A. 1976 Movement of solitary and periodic waves with an amplitude close to the limiting in a liquid layer of slowly varying depth. *Fluid Dyn.* **11**, 884–893.

KULIKOVSKII, A. G. REUTOV, V. A. 1980 Propagation of nonlinear waves above semi-infinite underwater troughs and ridges. *Fluid Dyn.* **15**, 217–224.

LAITONE, E. V. 1960 The second approximation to cnoidal and solitary waves. *J. Fluid Mech.* **9**, 430–444.

LIU, L. F. & YOON, S. B. 1986 Stem waves along a depth discontinuity *J. Geophys. Res.* **91**, 3979–3982.

LONGUET-HIGGINS, M. S. & FENTON J. D. 1974 On the mass, momentum, energy and circulation of a solitary wave II. *Proc. R. Soc. Lond.* A **340**, 471–493.

MILES, J. W. 1977*a* Obliquely interacting solitary waves. *J. Fluid Mech.* **79**, 157–169.

MILES, J. W. 1977*b* Resonantly interacting solitary waves. *J. Fluid Mech.* **79**, 171–179.

MILES, J. W. 1977*c* Diffraction of solitary waves. *Z. Angew. Math. Phys.* **28**, 889–902.

MILES, J. W. 1977*d* An axisymmetric Boussinesq wave *J. Fluid Mech.* **84**, 181–191.

MILES, J. W. 1980 Solitary waves. *Ann. Rev. Fluid Mech.* **12**, 11–43.

PEDERSEN, G. 1988 Three-dimensional wave patterns generated by moving disturbances at transcritical speeds. *J. Fluid Mech.* **196**, 39–63.

PEDERSEN, G. 1991 Finite difference representations of nonlinear waves. *Intl J. Num. Meth. Fluids* **13**, 671–690.

PEREGRINE, D. H. 1983 Wave jumps and caustics in the propagation of finite-amplitude water waves. *J. Fluid Mech.* **136**, 435–452.

PEREGRINE, D. H. 1985 Water waves and their development in space and time. *Proc. R. Soc. Lond.* A **400**, 1–18.

REUTOV, V. A. 1976 Behaviour of perturbations of solitary and periodic waves on the surface of a heavy liquid. *Fluid Dyn.* **11**, 778–781.

WHITHAM, G. B. 1974 *Linear and Nonlinear Waves.* Wiley-Interscience. New York.

WITTING, J. 1975 On the highest and other solitary waves. *SIAM J. Appl. Maths* **28**, 700–719.

WU, T. Y. 1981 Long waves in ocean and coastal waters. *Proc. ASCE. J. Engng. Mech. Div.* **107**, (EM3), 501–522.

YUE, D. K. P. & MEI, C. C. 1980 Forward diffraction of Stokes waves by a thin wedge. *J. Fluid Mech.* **99**, 33–52.